coatings

MDPI

Article

# Repetitive Impact Wear Behaviors of the Tempered 25Cr3Mo2NiWV Fe-Based Steel

**Cheng Zhang [1,†], Pu Li [1,†], Hui Dong [2,*], Dongliang Jin [1,*], Jinfeng Huang [3], Feng Mao [1] and Chong Chen [1]**

1 National Joint Engineering Research Center for Abrasion Control and Molding of Metal Materials, School of Materials Science and Engineering, Henan University of Science and Technology, Luoyang 471003, China; zhangch06@126.com (C.Z.); lp771597120@163.com (P.L.); maofeng718@163.com (F.M.); chenchong8812@163.com (C.C.)

2 School of Materials Science and Engineering, Xi'an Shiyou University, Xi'an 710065, China

3 State Key Laboratory for Advanced Metals and Materials, University of Science and Technology Beijing, Beijing 100083, China; ustbhuangjf@163.com

* Correspondence: donghui@xsyu.edu.cn (H.D.); ziranheping@163.com (D.J.); Tel.: +86-29-8838-2607 (H.D.); +86-731-6427-0020 (D.J.)

† These authors contributed equally to this work.

Received: 9 December 2019; Accepted: 23 January 2020; Published: 26 January 2020


**Abstract:** This study aimed to reveal the impact wear behaviors of tempered 25Cr3Mo2NiWV steel. The specimens were subject to various heat treatment processes for generating different mechanical and wear properties. The impact wear tests were performed with an MLD-10 dynamic abrasive wear tester. Worn surface morphologies and micro-cracks of the cross-sections were analyzed by optical microscope and scanning electron microscope. The Vickers hardness of the sample and the impact wear mechanism were also analyzed. The steel with the best combination of hardness and toughness had the lowest wear. With the increase of wear time, the dominant wear mechanism varied from slight plastic deformation to micro-cutting and adhesive wear. Finally, micro fatigue peeling occurred. After impact wear, the cracks could initiate from the surface or the sub-surface. Micrographs of the crack in the cross-section demonstrated two different propagation modes of fatigue fractures. The results showed that the strength and toughness of steel affected the crack propagation, surface spalling, and wear failure mechanism during impact wear.

**Keywords:** impact wear; steel; hardness; toughness; micro fatigue; cracks

## 1. Introduction

Die steel possesses proper hardness and toughness, good tempering resistance, and moderate cost; thus, it is widely utilized in the manufacturing industry [1]. Wear is one of the main causes of mechanical parts failure [2–6]. In working processes, cyclic mechanical loadings are applied to dies, finally leading to serious damage to the workpiece. The impact wear can alter the dimensional accuracy of the mold, and reduce the surface quality of machine parts, failing the production requirements. Moreover, the impact wear can cause mold fracture and shorten its service life. Therefore, the behavior of impact wear has become one of the important concerns for steel researchers [7–9].

Generally, the wear behavior of given steel has a close relationship with its heat-treatment process, hardness, and toughness [10]. Therefore, the researches on the effect of heat-treatment on the wear behavior are of importance to engineering. Heat treatment can change the mechanical properties of the steel and thus enhance their wear resistance [10–14]. To study the characteristics and the law of the impact wear failure of the test steel, it is tempered at different temperatures to produce various combinations of hardness and toughness.

The wear test is carried out for alloys with an dynamic abrasive wear tester (MLD-10, Zhangjiakou, China). In this test, the circular friction pair rotates under the testing machine. The specimen is fixed on the top, reciprocating up and down, and the repeated impact wear process is carried out within a set time.

Due to good hardenability and fatigue properties, the secondary hardening steel has been widely employed in mold manufacturing [1,15,16]. As an exploratory work [17], the previous research studied the effects of tempering temperature on mechanical properties, total weight loss, and surface morphology of one kind of secondary hardening steel. To obtain better comprehensive properties, the 25Cr3Mo2NiWV steel was developed through the adjustment of elements. On the basis of improved steel, the wear behaviors in different time stages, including weight loss, surface wear morphology, and wear mechanism, were studied more carefully. Besides, different types of cracks were found on the surface and sub-surface of the specimen. In this paper, the impact wear process in different periods was studied more deeply, which was more significant to understand the impact wear behavior of this kind of steel.

## 2. Experiment

### 2.1. Material and Heat Treatment

The chemical composition of the 25Cr3Mo2NiWV steel was 0.23 wt.% C, 0.06 wt.% Si, 2.97 wt.% Cr, 2.35 wt.% Mo, 1.05 wt.% Ni, 0.39 wt.% W, 0.27 wt.% V, and remainder Fe. The steel was prepared by vacuum melting combined with the electro-slag remelting process and forged by 400 kg air hammer into Φ70 mm bar stocks. The stable structure of the steel was obtained after annealing at 870 °C for 2 h. The austenitizing and tempering heat treatment conditions and mechanical properties of the steel are listed in Table 1. Due to the secondary hardening effect, the hardness of 25Cr3Mo2NiWV steel increased slightly when tempered at 550 °C [18].

The hardness of the tempered steel was obtained using a Rockwell hardness tester (HR150A, Shandong, China) with an applied load of 150 kg, and the applied load was 200 g for a Vickers hardness tester (HVS-1000A, Shandong, China). The impact toughness test was conducted on an impact test machine (JBDW-300D, Qingdao, China), and the impact specimen was a u-shaped notched sample with a size of 10 mm × 10 mm × 55 mm. All of the mechanical properties were averaged from three results with standard error within ±5% variation.

**Table 1.** Heat treatment conditions and mechanical properties of the steel.

| No. | Condition | Rockwell Hardness (HRC) | Impact Toughness ($J \cdot mm^{-2}$) |
|---|---|---|---|
| 1 | T1: austenitized at 980 °C for 1.5 h and quenching in water at room temperature, followed by tempering at 300 °C for 2 h | 45.9 ± 0.4 | 54.5 ± 3.7 |
| 2 | T2: same quenching as T1, tempering at 550 °C for 2 h | 46.7 ± 0.5 | 69.8 ± 3.2 |
| 3 | T3: same quenching as T1, tempering at 680 °C for 2 h | 32.3 ± 0.7 | 102.6 ± 3.4 |

### 2.2. Impact Wear Test

An MLD-10 impact tester was used to investigate the effect of mechanical properties on the impact wear resistance of the 25Cr3Mo2NiWV steel, as shown in Figure 1. The 10 kg impact hammer falling with a height of 4 mm corresponding to impact energy of 4 J was used for the tests without abrasive particles and lubricants. Impact frequencies and rotation frequencies were 200 times/min and 200 r/min, respectively. The upper specimen with the size of 10 mm × 10 mm × 30 mm was cut from the tempered bars, and the lower specimen was a quenched GCr15 steel with a size of Φ50 mm (hardness of 60 HRC).

The chemical composition of the GCr15 steel was 1.02 wt.% C, 1.59 wt.% Cr, 0.33 wt.% Si, 0.30 wt.% Mn, and remainder Fe.

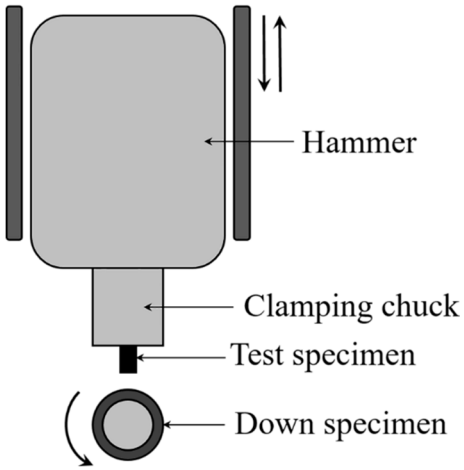


**Figure 1.** Schematic illustration of the MLD-10 impact wear tester.

Before wear tests, the specimen was ground by 600 grit silicon carbide paper, and then cleaned ultrasonically in the alcohol for 20 min. During the wear test, the specimens were weighed every 15 min using an electronic balance with an accuracy of 0.00001 g. The wear mass loss was average from three results for each period.

### *2.3. Microscopic Analysis*

The morphologies and chemical composition of the worn surface were analyzed via a scanning electron microscope (SEM, TESCAN-VEGA3SBH, Warrendale, PA, USA) and the energy spectrometer (EDS). The cross-section of the worn surface was ground using a final 2000 grit silicon carbide paper and then corroded with 8% nitric acid alcohol. The cracks in the cross-section were studied using optical microscopy (OM, OLYMPUS-BX51M, Tokyo, Japan) and SEM. The micro-hardness was tested three times on the cross-section by Vickers hardness tester (HVS-1000A, Shandong, China).

## 3. Results and Discussion

### *3.1. Wear Loss of 25Cr3Mo2NiWV Steel with Time*

Figure 2 shows the wear loss as a function of time for the steel tempered at different temperatures. The weight loss increased with time for all of the specimens. The weight losses of these three types of specimens increased slowly in the first 15 min. However, the increment of the wear loss increased rapidly after 15 min, which was caused by the rough surface from the microstructural aspect [19]. The real contact area was small between the upper and lower specimens during the initial stage of friction, only some undulations on the surface contacted with each other. With the proceeding of impact wear, the protrusions would undergo plastic deformation and adhesive tear under the impact force and shear stress when the stress is greater than the yield strength of the material [19,20]. The protrusions could partially break away from the wear system and result in weight loss, and the debris would form hard particles to cause micro-cutting.

The hardness of the tempered steel at 300 and 550 °C was higher than that tempered at 680 °C, resulting in a lower weight loss caused by micro-cutting during a long-time test. Due to higher hardness, the embedding of the hard particles that broke away from the steel surface was difficult, and its embedding depth was small under the impact force. Furthermore, the particles with shallow embedding depth that formed cutting effect could not slide long-distance on the steel surface, owing to the instantaneity of the impact load [21]. At the initial stage of the wear test for the steel tempered

at 680 °C, the particles were easy to be embedded into the matrix and plowed the steel surface by tangential friction [22]. However, the plowed metal could be rapidly pressed back into the steel matrix, resulting from the high plasticity and toughness of the matrix. Therefore, its wear loss was also low at the initial wear stage.

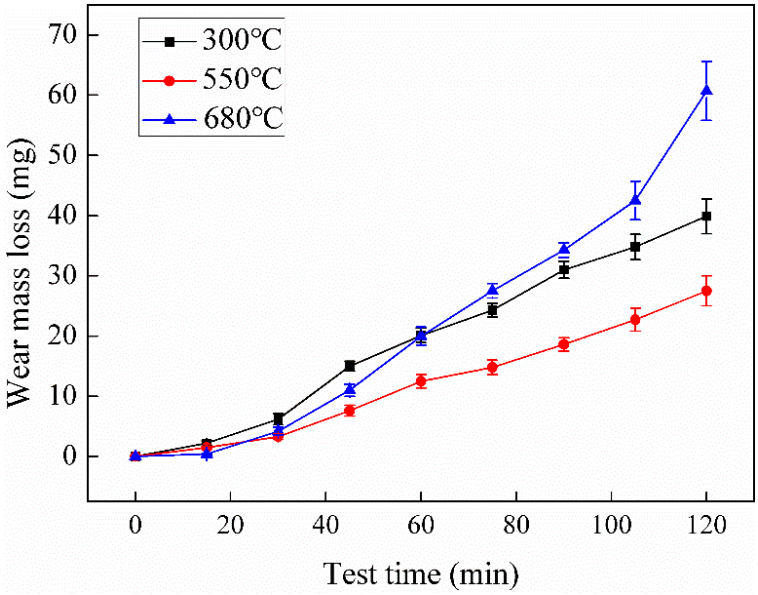


**Figure 2.** Weight loss as a function of wear time for the specimens tempered at different temperatures.

As the wear time increased, the ability of plastic deformation decreased for the steel surface, and the damage on the worn surface accumulated under the repeated impact. Cracks were generated by the large stress concentration in the grain boundary of the matrix, which could propagate and connect to form peeling during the test [23]. This might be the reason that the wear rate of the steels was higher after 15 min, as shown in Figure 2.

### *3.2. Evolution of the Worn Surface Morphology*

According to the results from Figure 2, the analysis of the wear mechanism was mainly focused on the steel tempered at 680 °C due to its highest wear loss. Figure 3 shows the surface morphologies of the steel tempered at 680 °C with different wear times. The worn surface was relatively flat after the impact test for 5 min. The slight impact indentation was uniformly distributed on the surface, and some adhesive marks are presented in Figure 3a. The surface appeared obvious plastic deformation after a 10-min test, as shown in Figure 3b. The small protrusions could act as hard abrasive particles at the early stage of wear and scratch the surface under the impact load, resulting in some grooves with adhesive tear marks [24,25]. The wear mechanisms were mainly micro-cutting. With the increasing time, serious plastic deformation appeared on the surface, the widths and the depths of the grooves were expanded, leading to an increase of the wear loss. At the same time, the material in the groove could be pushed onto both sides of the groove to form a plastic ridge [26,27]. Besides, the scale-shaped morphology could be seen because of severe adhesive wear [28], and sheet-shaped debris with a size of ~15 μm could be observed locally, as shown in Figure 3c.

Figure 4 shows the surface morphology and EDS analysis of 25Cr3Mo2NiWV steel after tempering at 680 °C and wear test for 15 min. The contents of C and Si elements in the grinding material (GCr15) were higher than those of 25Cr3Mo2NiWV steel. During the adhesive wear, a part of the asperities on the surface of grinding material was torn and transferred to the worn surface of the impact specimen. In Figure 4, the content of C and Si elements in the adhesive wear area was higher, proving the adhesive features. Besides, the impact wear could rise the local temperature of the sample surface, leading

to oxidation. The oxygen content in the adhesion region was higher, which was consistent with the results of So [29].

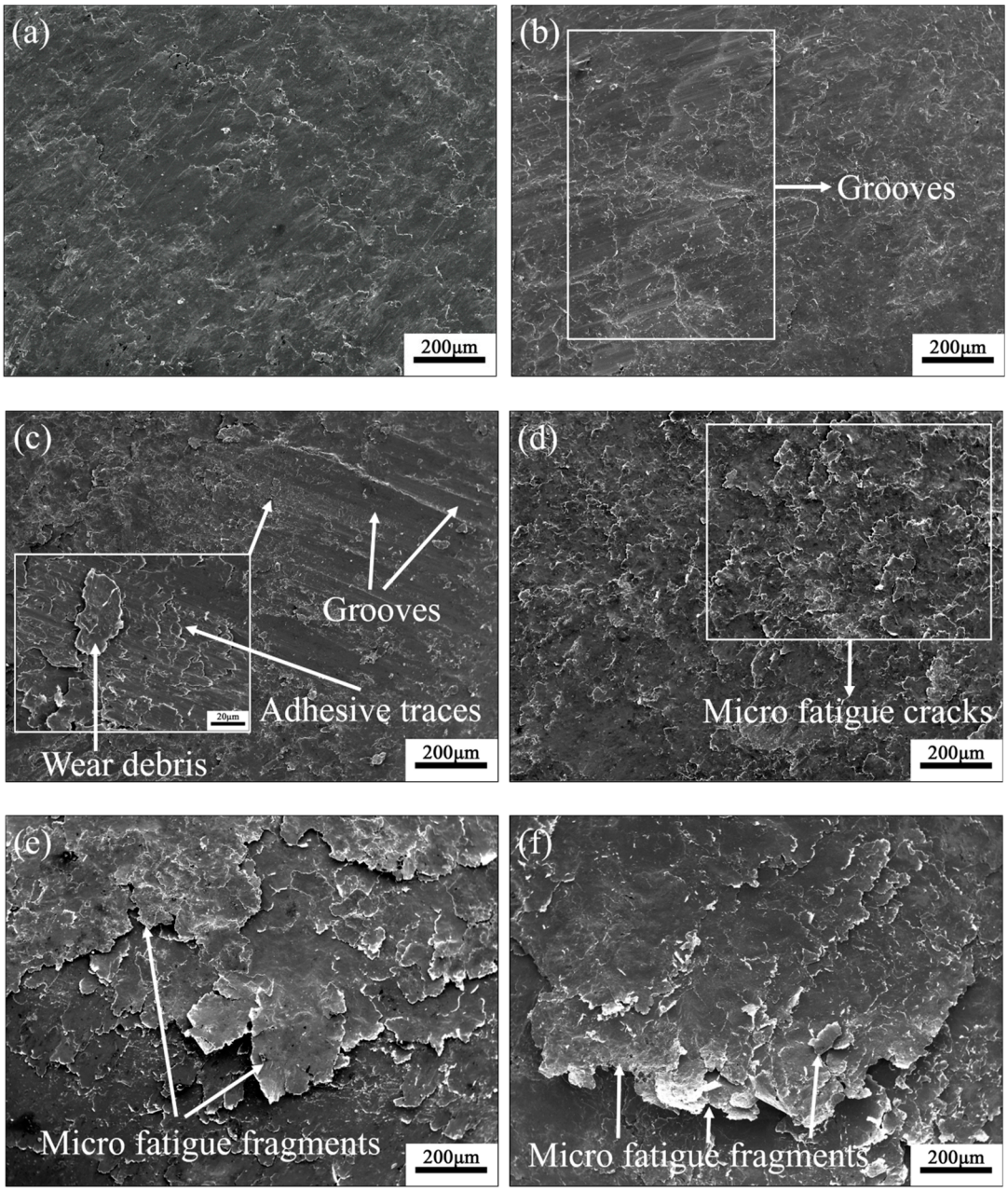


**Figure 3.** Surface morphologies of the steel tempered at 680 °C for different impact wear times, (**a**) 5 min; (**b**) 10 min; (**c**) 15 min; (**d**) 30 min; (**e**) 60 min; (**f**) 120 min.

At 30 min, no signs of adhesive wear were presented on the steel surface, while after frequent dynamic impact on the sample surface, a large number of micro fatigue cracks were observed, as shown in Figure 3d. There were mainly two reasons for the formation of the micro fatigue cracks. Firstly, the micro friction traces after adhesive wear become micro-cracks under the impact force and then propagate to form micro fatigue cracks [30]. Secondly, the deformation degree of the plastic ridge on both sides of the groove increases and transforms into an extrusion hardening ridge under repeated impact. The root of the hardened edge is prone to crack due to strain fatigue [31].

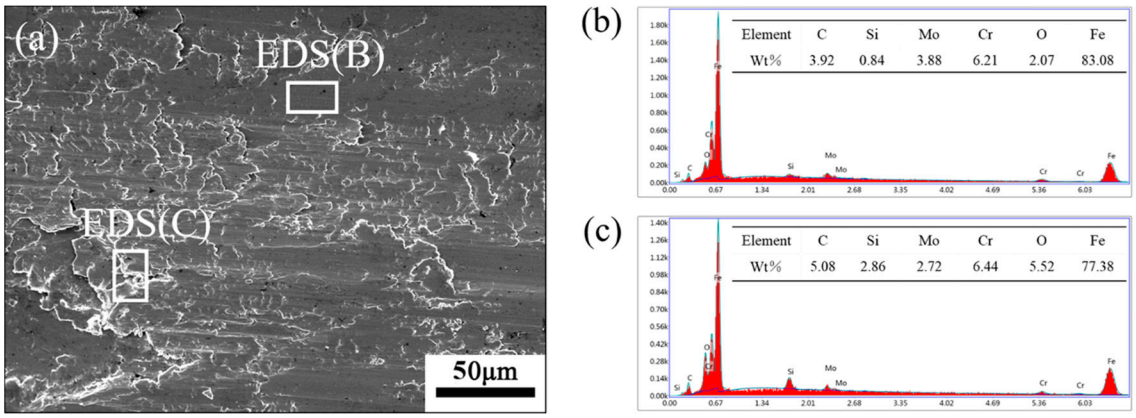


**Figure 4.** Surface wear morphology and EDS analysis of 680 °C tempered samples after 15 min wear. (**a**) Micro morphology of worn surface; (**b**) EDS analysis of region marked with EDS(B); (**c**) EDS analysis of region marked with EDS(C).

For the 60-min wear test, the worn surface was hardened under the impact, and the fatigue crack was easier to develop. It could be seen that small cracks propagated and coalesced to form large cracks, and the lip at the front of the fragment had the potential to peel off under the shear stress, as shown by the arrow in Figure 3e. At the 120-min test, the surface morphology was quite rough, filled with fish-scale fragments, as shown in Figure 3f. There were fractures between the fatigue fragments, and the wear mechanism was mainly micro fatigue peeling wear.

Besides, based on the morphologies in Figure 3, it also could be deduced that the hardness and the toughness of the 25Cr3Mo2NiWV steel both dramatically affected its impact wear resistance. Due to high hardness, the depth and width of the groove were small, and the weight loss by micro-cutting was correspondingly low. With high toughness, the fatigue crack was not easily formed, resulting in the fatigue peeling under the impact wear [32]. Therefore, the high hardness and toughness were beneficial to promote the wear resistance of the steel.

During the wear test of the 25Cr3Mo2NiWV steel, the dominant wear mechanisms varied from the slight plastic deformation to micro-cutting and adhesive wear, finally to micro fatigue peeling wear in the dynamic impact wear. Due to the different hardness and toughness, the main wear mechanism varied with the different specimen surface in the same wear time, leading to different wear weight losses.

### *3.3. Effects of Tempering Temperature on the Worn Surface Morphologies*

Figure 5 displays the worn surface morphologies of the steels with different tempering temperatures after wear for a different time. The typical fish-scale fragments were observed on all surfaces. The surface was the flattest for the specimen tempered at 550 °C with the wear time of 60 min, and no fatigue peeling presents in Figure 5(b1). The worn surfaces of the steels tempered at 300 and 680 °C were quite rough, and the size of the fragments was large, as shown in Figure 5(a1,c1). The fish scale fractures along the direction of shear stress and the secondary micro-cracks could be observed, which indicated that a large part of fish scales had peeled off, resulting in weight loss and poor wear resistance.

For 120 min wear time, the surface morphologies of all specimens were almost the same as those worn for 60 min, but their fatigue peeling was more serious, as shown in Figure 5(a2,c2). Except for the steel tempered at 550 °C, the worn sub-surface layer had been exposed for the other specimens, as marked as 2 in Figure 5 (the area marked as 1 is the initial wear surface). The surface temperature of the specimens could rise owing to impact and friction, decreasing the wear resistance of the surface layer. Besides, due to the low strength and hardness of the steel tempered at 680 °C, its surface morphology was the roughest with the largest peeling off, and the plastic extrusion was found on the cross-section [33], as shown in Figure 6.

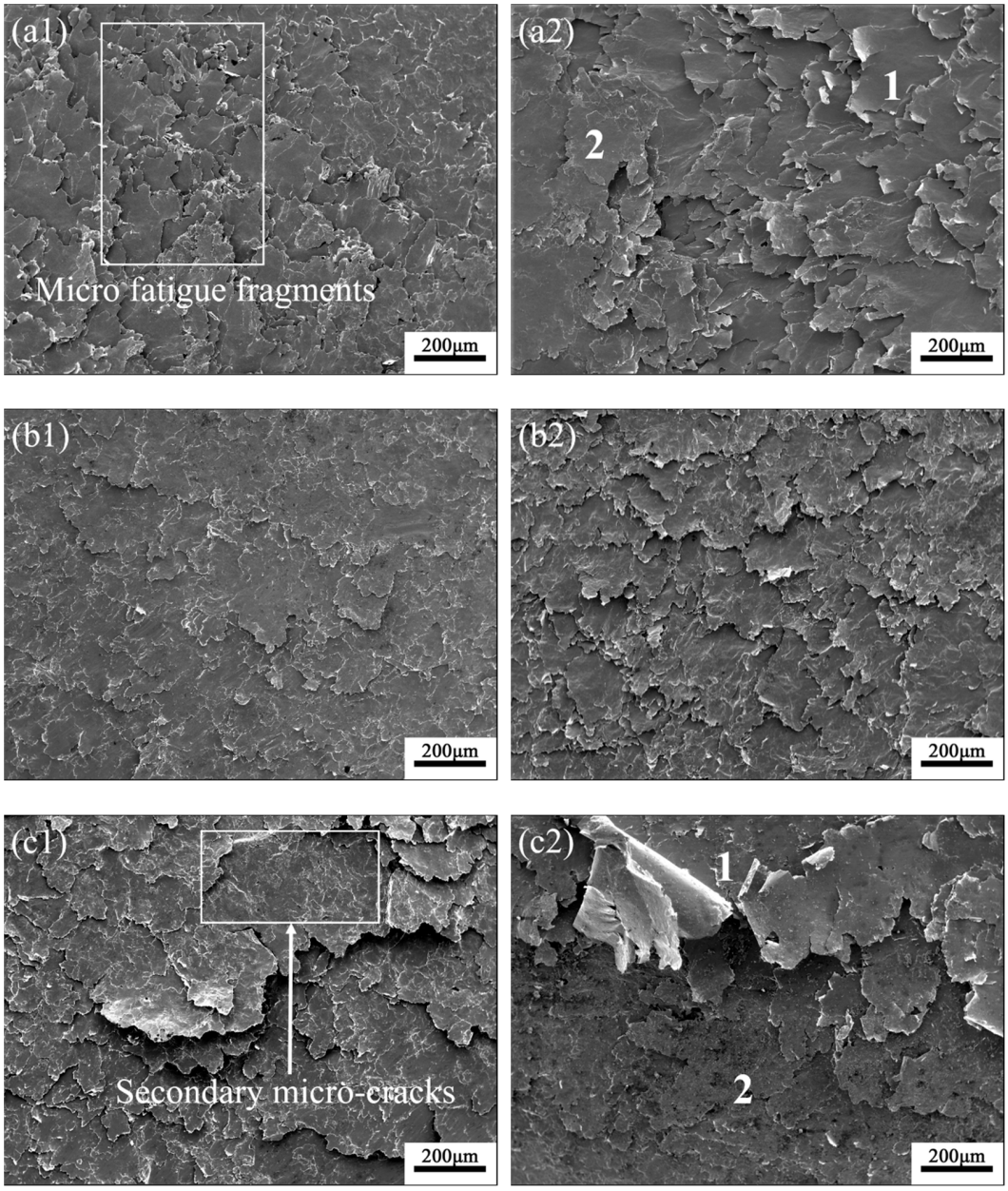


**Figure 5.** Worn surface morphologies of the tempered steels, (**a1**) 300 °C/60 min and (**a2**) 300 °C/120 min; (**b1**) 550 °C/60 min and (**b2**) 550 °C/120 min; (**c1**) 680 °C/60 min and (**c2**) 680 °C/120 min.

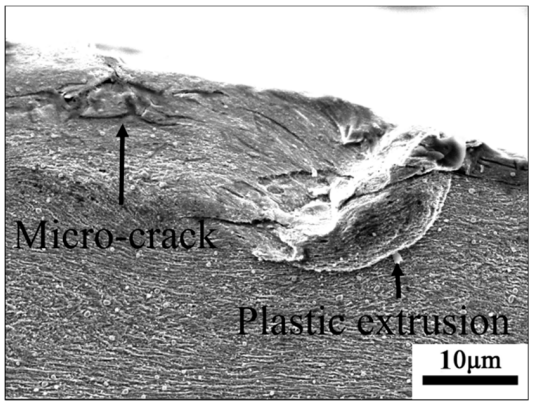


**Figure 6.** Cross-section morphology of the steel tempered at 680 °C after impact wear for 120 min.

### *3.4. Mechanism of Crack Initiation and Surface Spalling*

Essentially, wear is the process of hardening and peeling off in the worn surface, that is, the process of forming, expanding, and converging of micro-cracks in the surface layer [34]. Table 2 shows the micro-hardness of the cross-sections of the steels tempered at different temperatures. The surface layer experiences serious plastic deformation after impact wear; thus, its hardness is higher than that of the metal matrix.

**Table 2.** Micro-hardness of surface layer and matrix after wear tests.

| Condition | None Heat Treatment | Tempering Temperature (°C) | | |
|---|---|---|---|---|
| | | 300 | 550 | 680 |
| Matrix hardness (HV) | 151.0 ± 3.1 | 439.3 ± 5.5 | 458.0 ± 6.0 | 292.3 ± 7.6 |
| Surface hardness (HV) | – | 589.0 ± 5.3 | 572.0 ± 6.2 | 418.0 ± 9.6 |
| Hardness difference (HV) | – | 149.7 ± 2.1 | 114.0 ± 1.7 | 125.7 ± 2.5 |

Figure 7 presents the micrographs of the crack in the cross-section, demonstrating two different propagation modes of the fatigue fractures.

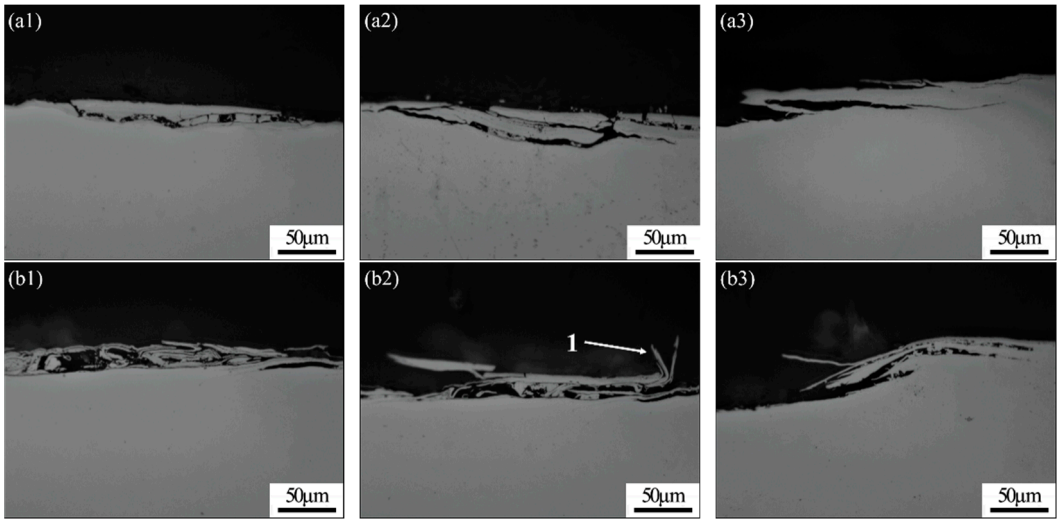


**Figure 7.** Cross-sectional micrographs of the steels after wear for 120 min. (**a1**–**a3**) Steel tempered at 300 °C, brittle fatigue fractures; (**b1**–**b3**) steel tempered at 680 °C, ductile fatigue fractures.

Cracks initiated on the worn surface under impact load (Figure 7(a1,b1)) and then expanded and converged at a small angle into the matrix, finally returning to the surface to cause flake spalling in Figure 7(a2,b2), exposing the sub-surface layer. The cracks in the steel tempered at 300 °C were straight with clear edges in Figure 7(a1,a3), showing a brittle fracture due to high hardness and low toughness. Combined with work hardening, the surface became harder and more brittle, obstructing the stress release and aggravating the expansion of fatigue cracks. The difference of the micro-hardness between the surface and matrix for the steel tempered at 300 °C was the largest, 149.7 HV, indicating poor coordination between the surface and the matrix. Once the fatigue crack initiated, it would expand rapidly along with the surface layer under the shear stress, ultimately causing the surface layer to peel off.

The cross-section of the worn steel tempered at 680 °C is shown in Figure 7(b1,b3). The higher tempering temperature induced a higher toughness, and the resistance to crack propagation was enhanced. Consequently, the cracks were short and curved, showing a plastic fracture mode. However, the higher tempering temperature decreased the strength of the metal matrix, leading to low resistance to plastic deformation. The micro-cracks were more easily to initiate from the grooves under impact

load [35]. Besides, the fatigue scaling marked by arrow 1 in Figure 7(b2) did not break away during impact wear, also indicating a plastic fracture mechanism. The plastic scale could be folded before peeling off, as shown in Figure 5(c2).

After the test, the surface cracks and spalling of the specimen tempered at 550 °C were less, as shown in Figure 5(b1,b2). The crack initiation and propagation were evident.

Figure 8 shows the different micro-cracks in the cross-sections of the steels tempered at 550 °C after impact wear for a different time. Under the normal and shear stress, severe plastic deformation developed in the surface layer, forming the typical streamline under high strain [36].

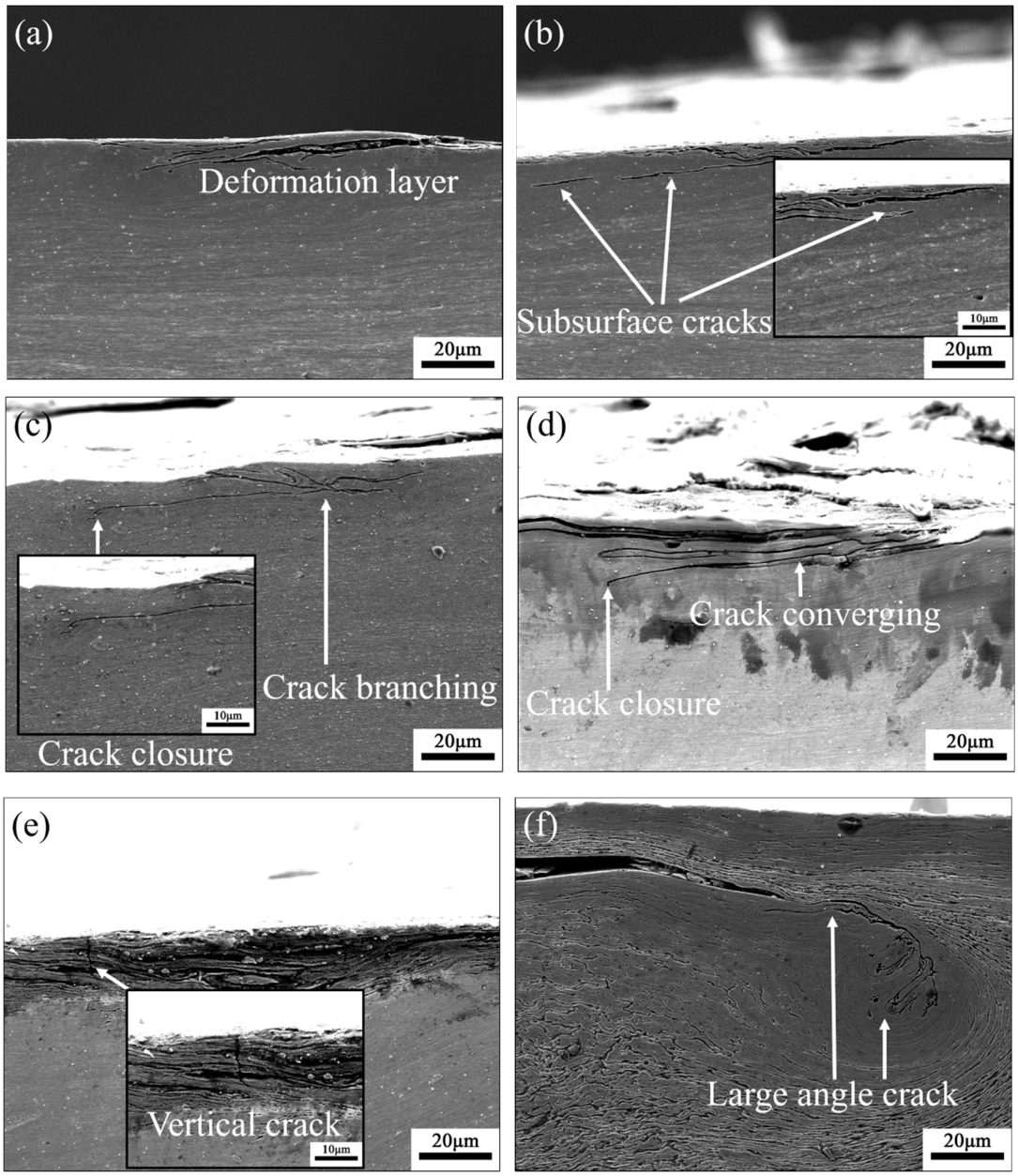


**Figure 8.** Micro-cracks in the cross-sections of the steels tempered at 550 °C after wear for different time, (**a**) 30 min, crack expanding inward; (**b**) 30 min, sub-surface crack expanding outwards; (**c**) 60 min, crack propagating; (**d**) 60 min, crack converging; (**e**) 120 min, vertical crack; (**f**) 120 min, sub-surface large-angle crack.

Cracks in the dense streamline could expand inward (Figure 8a) and outward (Figure 8b) and produce branches (Figure 8c), even converge to form a long curved crack (Figure 8d). These kinds of

cracks were mainly initiated along with the interface of martensitic. The cracks near the surface almost expanded parallel to the surface.

From Figure 8b,d, it could be found that the expansion of the cracks near the surface paused after branching in the metal matrix. Moreover, the cracks near the surface could be closed by large compressive stress [37]. Figure 8e shows a vertical crack without branching in the surface layer. The vertical cracks often converged with the crack parallel to the surface. Figure 8f presents a large angle crack formed in the sub-surface. According to the fatigue theory [38], when the metal material is impacted, the micro defects, such as dislocations, first form in the sub-surface under the impact, and then evolve into cracks, finally resulting in spalling. However, the lath of the martensite has a high density of dislocations, which could form a large number of dislocation tangles and dislocation walls during impact wear [39,40], leading to the development of the large angle crack, as shown in Figure 8f.

## 4. Conclusions

Both hardness and toughness could affect the wear properties of steel. Hardness has a greater influence on wear properties. The steel with the best combination of hardness and toughness has the lowest wear weight loss.

With the increase of wear time, the dominant wear mechanisms of all tempered steels vary from the slight plastic deformation to micro-cutting and adhesive wear, finally to micro fatigue peeling wear. Due to the different hardness and toughness, the main wear mechanism of three tempered specimens are different during the same wear time, resulting in different wear weight losses.

During impact wear, the fatigue cracks could initiate from the surface and the sub-surface, and then propagate and converge to form fatigue delamination. The fatigue cracks in the cross-section show the characteristics of the toughness and brittleness. The brittle fatigue fractures mainly appear in the steels with high hardness. However, the ductile fatigue fractures mainly occur in the steels with high toughness. With a good combination of strength and toughness, the surface cracks and spalling of the specimen are the least.

**Author Contributions:** Conceptualization and investigation, C.Z.; data curation and investigation, P.L.; writing—review and editing, H.D.; writing—original draft, D.J.; formal analysis, J.H.; data curation, F.M.; investigation, C.C. All authors have read and agreed to the published version of the manuscript.

**Funding:** The work was supported by the National Key R&D Program of China (No. 2016YFB0300701), Key Scientific and Technological Project of Henan Province (Nos. 182102210043 and 192102210009).

**Conflicts of Interest:** The authors declare no conflict of interest.

## References

1. Zhu, Z.Y. Property data collection of common hot working die steels used in China. *Mater. Mech. Eng.* **2001**, *26*, 42–46.
2. Koiprasert, H.; Dumrongrattana, S.; Niranatlumpong, P. Thermally sprayed coatings for protection of fretting wear. *Wear* **2004**, *257*, 1–7. [CrossRef]
3. Jiang, Z.; Mao, Z.; Zhang, Y.; Zhang, J. A study on dynamic response and diagnosis method of the wear on connecting rod bush. *J. Fail. Anal. Prev.* **2017**, *17*, 812–822. [CrossRef]
4. Wei, S.; Xu, L. Review on research progress of steel and iron wear-resistant material. *Acta Metall. Sin.* **2019**. [CrossRef]
5. Luong, L.H.S.; Heijkoop, T. The influence of scale on friction in hot metal working. *Wear* **1981**, *71*, 93–102. [CrossRef]
6. Barrau, O.; Boher, C.; Gras, R.; Rezai-Aria, F. Analysis of the friction and wear behavior of hot work tool steel for forging. *Wear* **2003**, *255*, 1444–1454. [CrossRef]
7. Liu, Y.; Janssen, G.C.A.M. Impact wear of structural steel with yield strength of 235 MPa in various liquids. *Coatings* **2017**, *7*, 237. [CrossRef]
8. Yilmaz, H.; Sadeler, R. Impact wear behavior of ball burnished 316L stainless steel. *Surf. Coat. Technol.* **2019**, *363*, 369–378. [CrossRef]

9. Wang, Z.; Cai, Z.; Sun, Y.; Peng, J.; Zhu, M. Low velocity impact wear behavior of MoS2 /Pb nanocomposite coating under controlled kinetic energy. *Surf. Coat. Technol.* **2017**, *326*, 53–62. [CrossRef]
10. Cui, X.H.; Wang, S.Q.; Wei, M.X.; Yang, Z.R. Wear characteristics and mechanisms of H13 steel with various tempered structures. *J. Mater. Eng. Perform.* **2011**, *20*, 1055–1062. [CrossRef]
11. Xu, L.; Wei, S.; Xiao, F.; Zhou, H.; Zhang, G.; Li, J. Effects of carbides on abrasive wear properties and failure behaviors of high speed steels with different alloy element content. *Wear* **2017**, *376–377*, 968–974. [CrossRef]
12. Xu, L.; Xiao, F.; Wei, S.; Liu, D.; Zhou, H.; Zhang, G.; Zhou, Y. Microstructure and wear properties of high-speed steel with high molybdenum content under rolling-sliding wear. *Tribol. Int.* **2017**, *116*, 39–46. [CrossRef]
13. Xu, L.; Wei, S.; Xing, J.; Long, R. Effects of carbon content and sliding ratio on wear behavior of high-vanadium high-speed steel (HVHSS) under high-stress rolling sliding contact. *Tribol. Int.* **2014**, *70*, 34–41. [CrossRef]
14. Xu, L.; Wei, S.; Han, M.; Long, R. Effect of carbides on wear characterization of high-alloy steels under high-stress rolling-sliding condition. *Tribol. Trans.* **2014**, *57*, 631–636. [CrossRef]
15. Hao, X.; Pan, M.L; Liu, X.F. Effect of cerium on microstructure and wearing resistance of 5CrMnMo hot working die steel. *Adv. Mater. Res.* **2011**, *284–286*, 1615–1620. [CrossRef]
16. Kuang, J.X.; Wang, X.H.; Liu, A.M.; Zhu, H.S. Study on the complex strengthening processes of 5Cr2NiMoVSi steel large hot forging dies. *Adv. Mater. Res.* **2011**, *189–193*, 1056–1061. [CrossRef]
17. Zhang, C.; Li, P.; Wei, S.; You, L.; Wang, X.; Mao, F.; Jin, D.; Chen, C.; Pan, K.; Luo, C.; et al. Effect of tempering temperature on impact wear behavior of 30Cr3Mo2WNi hot-working die steel. *Front. Mater.* **2019**, *6*, 149. [CrossRef]
18. Chen, X.F.; Yao, Z.H.; Huang, J.F.; Zhang, J.; Dong, J.X. Thermodynamic calculation of precipitated phase in 25Cr3Mo2NiWVNb steel. *China Sciencepaper* **2017**, *12*, 1178–1183.
19. Jahanmir, S.; Suh, N.P.; Abrahamson, E.P., II. Abrahamson. The delamination theory of wear and the wear of a composite surface. *Wear* **1975**, *32*, 33–49. [CrossRef]
20. Wei, M.; Wang, S.; Wang, L.; Chen, K. Effect of microstructures on elevated-temperature wear resistance of a hot working die steel. *J. Iron Steel Res. Int.* **2001**, *18*, 47–53. [CrossRef]
21. Bialobrzeska, B.; Kostencki, P. Abrasive wear characteristics of selected low-alloy boron steels as measured in both field experiments and laboratory tests. *Wear* **2015**, *328–329*, 149–159. [CrossRef]
22. Wang, X.; Chen, Y.; Wei, S.; Zuo, L.; Mao, F. Effect of carbon content on abrasive impact wear behavior of Cr-Si-Mn low alloy wear resistant cast steels. *Front. Mater.* **2019**, *6*, 153. [CrossRef]
23. Laird, G., II; Collins, W.K.; Blickensderfer, R. Crack propagation and spalling of white cast iron balls subjected to repeated impacts. *Wear* **1988**, *124*, 217–235. [CrossRef]
24. Archard, J.F.; Hirst, W. The wear of metals under unlubricated conditions. *Proc. Math. Phys. Eng. Sci.* **1956**, *236*, 397–410.
25. Xu, J. Study on the coated tool disability and the work-piece surface quality in high speed cutting. *Key Eng. Mater.* **2010**, *431–432*, 397–400. [CrossRef]
26. Liu, C.-H.; Sun, G.-D.; Xiong, L.; Yang, X.-Q. Effect of heat treatment process on impact wear property and mechanism of SKD11 steel. *J. Iron Steel Res.* **2018**, *30*, 199–205.
27. Ding, H.; Cui, F.; Du, X. Effect of component and microstructure on impact wear property and mechanism of steels in corrosive condition. *Mater. Sci. Eng. A* **2006**, *421*, 161–167. [CrossRef]
28. Wei, M.X.; Wang, S.Q.; Wang, L.; Cui, X.H.; Chen, K.M. Effect of tempering conditions on wear resistance in various wear mechanisms of H13 steel. *Tribol. Int.* **2011**, *44*, 898–905. [CrossRef]
29. So, H.; Yu, D.S.; Chuang, C.Y. Formation and wear mechanism of tribo-oxides and the regime of oxidational wear of steel. *Wear* **2002**, *253*, 1004–1015. [CrossRef]
30. Sasada, T.; Oike, M.; Emori, N. The effect of abrasive grain size on the transition between abrasive and adhesive wear. *Wear* **1984**, *97*, 291–302. [CrossRef]
31. Dai, P.Q.; Huang, S.X. Effect of heat treatment on the impact abrasive wear resistance of medium carbon alloy steel. *Heat Treat. Met.* **1998**, *12*, 19–21.
32. Fricke, R.W.; Allen, C. Repetitive impact wear of steels. *Wear* **1993**, *162–164*, 837–847. [CrossRef]
33. So, H.; Chen, H.M.; Chen, L.W. Extrusion wear and transition of wear mechanisms of steel. *Wear* **2008**, *265*, 1142–1148. [CrossRef]
34. Rastegar, V.; Karimi, A. Surface and subsurface deformation of wear-resistant steels exposed to impact wear. *J. Mater. Eng. Perform.* **2014**, *23*, 927–936. [CrossRef]

35. Huang, J.F.; Fang, H.-S.; Xu, P.; Zheng, Y.K. Effect of Si on wear resistance of bainitic cast steel under high stress impact. *J. Iron Steel Res.* **2001**, *13*, 40–45.
36. Alpas, A.T.; Embury, J.D. The role of subsurface deformation and strain localization on the sliding wear behaviour of laminated composites. *Wear* **1991**, *146*, 285–300. [CrossRef]
37. Yang, Y.-Y.; Fang, H.-S.; Zheng, Y.-K; Yang, Z.-G.; Jiang, Z.-L. The failure models induced by white layers during impact wear. *Wear* **1995**, *185*, 17–22. [CrossRef]
38. Suh, N.P. An overview of the delamination theory of wear. *Wear* **1977**, *44*, 1–16. [CrossRef]
39. Peng, S.; Song, R.; Sun, T.; Yang, F.; Deng, P.; Wu, C. Surface failure behavior of 70Mn martensite steel under abrasive impact wear. *Wear* **2016**, *362–363*, 129–134. [CrossRef]
40. Peng, S.; Song, R.; Sun, T.; Pei, Z.; Cai, C.; Feng, Y.; Tan, Z. Wear behavior and hardening mechanism of novel lightweight Fe–25.1Mn–6.6Al–1.3C steel under impact abrasion conditions. *Tribol. Lett.* **2016**, *64*. [CrossRef]